Biosensors and Bioelectronics 44 (2013) 222–228

Contents lists available at SciVerse ScienceDirect

Biosensors and Bioelectronics

journal homepage: www.elsevier.com/locate/bios

Rapid, quantitative, reverse transcription PCR in a polymer microfluidic chip

D. Curtis Saunders, Gregory L. Holst, Christopher R. Phaneuf*, Nikita Pak, Matthew Marchese, Nicholas Sondej, Michael McKinnon, Craig R. Forest

G.W. Woodruff School of Mechanical Engineering, Georgia Institute of Technology, 315 Ferst Drive, Atlanta, GA 30332, USA

ARTICLE INFO

Article history:
Received 31 October 2012
Received in revised form
31 December 2012
Accepted 9 January 2013
Available online 18 January 2013

Keywords:
Microfluidics
Gene expression
Quantitative PCR
Radiative heating
Stem cells
Heat transfer

ABSTRACT

Quantitative PCR (qPCR) techniques have become invaluable, high-throughput tools to study gene expression. However, the need to measure gene expression patterns quickly and affordably, useful for applications such as stem cell biomanufacturing requiring real-time observation and control, has not been adequately met by rapid qPCR instrumentation to date. We report a reverse transcription, microfluidic qPCR system and its application to DNA and RNA amplification measurement. In the system, an environmental control fixture provides mechanical and thermal repeatability for an infrared laser to achieve both accurate and precise open-loop temperature control of 1 μl reaction volumes in a low-cost polymer microfluidic chip with concurrent fluorescence imaging. We have used this system to amplify serial dilutions of λ-phage DNA (10^5–10^7 starting copies) and RNA transcripts from the GAPDH housekeeping gene (5.45 ng total mouse embryonic stem cell RNA) and measured associated standard curves, efficiency (57%), repeatability (~1 cycle threshold), melting curves, and specificity. This microfluidic qRT-PCR system offers a practical approach to rapid analysis (~1 h), combining the cost benefits of small reagent volumes with the simplicity of disposable polymer microchips and easy setup.

1. Introduction

Gene expression measurement is an essential tool for molecular biology studies. For example, understanding gene expression patterns is fundamental to the study of mechanisms underlying stem cell pluripotency and self-renewal (Boyer et al., 2005; Sperger et al., 2003). A variety of tools have been developed for quantitative gene expression analysis across many genes and many cells. DNA microarrays allow one to probe virtually the entire transcriptome (Anon., 2006) and have become widely used in profiling expression of hundreds to hundreds of thousands of genes (Schena et al., 1995), although results can be noisy (Liang, 2007; Spurgeon et al., 2008). Fluorescence in situ hybridization (FISH) is commonly used when knowledge about the spatial distribution of gene expressions in cells or tissues is necessary and has been done in fixed (Itzkovitz and van Oudenaarden, 2011) and live (Santangelo et al., 2009) cells and has been advanced further using quantum dots (Bao et al., 2009) and fluorescent tags (Santangelo et al., 2004). However, scalability of this technology to multiple genes in multiple cells and tissues is hindered by expensive equipment and the need for long recording times and high-intensity illumination (Itzkovitz and van Oudenaarden, 2011). RNA sequencing technologies can be used to map a sample with no prior knowledge of the sample's genome by directly counting number of reads (Malone and Oliver, 2011), albeit at relatively high cost and long measurement duration.

The limited sensitivity, slow turnaround, and high costs of these techniques have led to the common practice of gene expression profiling with quantitative, reverse transcription, polymerase chain reaction (qRT-PCR; Dahl et al., 2007). This technique, widely regarded as the "gold standard," allows for highly specific, sensitive, and reproducible RNA quantification with a high dynamic range by reverse transcribing RNA into DNA and then exponentially amplifying the target sequence from as little as a single copy by thermal cycling, or thermocycling, a biochemical cocktail.

Miniaturized, or microfluidic, PCR systems have focused primarily on either increasing the number of genes able to be simultaneously measured (Dahl et al., 2007; Spurgeon et al., 2008), increasing the sensitivity of the system to single-cell analyses (Sanchez-Freire et al., 2012; Stahlberg and Bengtsson, 2010; White et al., 2011; Zare and Kim, 2010; Zeng et al., 2010; Zhong et al., 2007, 2008), or developing systems with sample-in answer-out capabilities (Cao et al., 2012; Easley et al., 2006; Kaigala et al., 2008; Lien et al., 2007; Liu et al., 2007; Wooley et al., 1996). Reports of large sample arrays (Dahl et al., 2007;

* Corresponding author. Tel.: +1 760 464 9745.
E-mail address: christopher.phaneuf@gatech.edu (C.R. Phaneuf).

0956-5663/$ - see front matter © 2013 Elsevier B.V. All rights reserved.
http://dx.doi.org/10.1016/j.bios.2013.01.019

Spurgeon et al., 2008; Warren et al., 2006) of sub-microliter reaction chambers have been published for high-throughput qRT-PCR that amplify as few as five starting copies of RNA in each chamber, effectively bridging the gap between the high-throughput capabilities of microarrays and the sensitivity of qPCR (Dahl et al., 2007). In addition, researchers have worked to expand the spatial frequency of single-cell analysis by separating and measuring the gene expression of 300 single cells simultaneously (White et al., 2011).

While these tools are powerful, they require hours or days per analysis. However, gene's expression patterns can change across a broad range of timescales, from slow events during development and pathogenesis (i.e., hours to days) to rapid responses to environmental signals (i.e., minutes to hours; Lopez-Maury et al., 2008; Stahlberg and Bengtsson, 2010; Yosef and Regev, 2011). If the measurement frequency can approach the gene expression timescales, real-time observation and intervention become possible. There is therefore a need for technologies capable of high temporal frequency sampling, governed by the Nyquist rate, to measure gene expression kinetics in single cells or cell populations in real time.

For rapid qPCR, Roche has developed a convective thermocycler that uses 10–50 μl reaction volumes for gene expression analysis in about 1 h (Wittwer et al., 1997), as compared to 2–3 h for conventional conductive thermocyclers (Erlich et al., 1991). Yu et al. (2012) report an infrared lamp-mediated microfluidic qPCR system following on a prior PCR innovation (Huhmer and Landers, 2000). Such devices enable rapid qPCR and PCR in a glass microfluidic device using a broadband infrared source in about 30 min. They hold much promise for performing other amplification strategies such as multiplex PCR or isothermal amplification or in combination with numerous pre- and post- PCR processes, allowing a highly integrated system. Others have implemented droplet thermocyclers, which use sub-microliter sample volumes and can perform qPCR in less than 10 min (Kim et al., 2009; Neuzil et al., 2006).

Coherent, infrared radiation-mediated thermocycling in a polymer microchip offers great potential for rapid gene expression measurement. By selecting a radiation frequency matched to the absorption spectra of the aqueous PCR reaction chemistry, efficient heat transfer directly to the microchip chamber is possible (Phaneuf et al., 2011). Advantages of this approach are high heat transfer rates, unfettered optical access, and low power consumption for compact instrumentation or exponential scaling.

We previously reported an open-loop, microfluidic "plug-and-play" PCR system capable of amplifying λ-phage DNA in 1 μl disposable polymer microchips in 10 min (Pak et al., 2012). This system is simple and easy-to-use like a conventional PCR instrument in that the user simply loads the sample into the microchip, installs it in the instrument, and removes it following amplification, in contrast to virtually all other reported microfluidic PCR instruments that require features such as valves, pumps, and temperature sensors (Oosterbroek and Berg, 2003). The reaction volume is sufficiently small for low reagent consumption, while being practical to interface with routine equipment (e.g., pipettes, reagent kits, and electrophoretic instrumentation). The PCR mixture utilizes common reagent concentrations, including the relatively costly polymerase enzyme (0.02–0.025 U/μl), unlike most reported microfluidic PCR that require 2–20× more (Angione et al., 2012; Cao et al., 2012; Hua et al., 2010). We attribute this advantage to the effectiveness of our passivation method (Phaneuf et al., 2012). The disposable polymer microchip is low-cost and more rapidly fabricated at relevant quantities (tens to thousands) than comparable glass or silicon devices (Becker and Gärtner, 2008; Oosterbroek and Berg, 2003). This easy-to-use system was designed for use with traditional end-point DNA detection techniques and targeted applications such as disease diagnostics.

However, for qRT-PCR, the accuracy and reproducibility of amplification are paramount and we therefore implemented substantial improvements in thermal, mechanical, and biological stability. We now report a microfluidic qPCR system and its application to both DNA and RNA measurement.

2. Materials and methods

The rapid, open loop system for qRT-PCR in a polymer microfluidic chip is shown in Fig. 1. The system consists of a microfluidic device featuring a 1 μl reaction chamber, an infrared laser system to thermocycle PCR in this chamber, an environmental control fixture for precise mechanical, thermal, and pressure stability, and a microscope for fluorescence detection.

2.1. Microfluidic device

The microchip (Fig. 1b,c) comprises two $20 \times 12.5 \times 1.5\ mm^3$ poly(methyl methacrylate) (PMMA) layers that are thermally bonded, 1.6 mm diameter alignment holes for repeatable positions, and a single 1 μl reaction chamber (500 μm wide, 800 μm deep, and 2.5 mm average length) accessed via 700 μm diameter fill ports and 250 μm wide × 190 μm deep channels. The chamber length was tapered such that the feature is trapezoidal to minimize bubble trapping. The 1.5 mm substrate thickness was

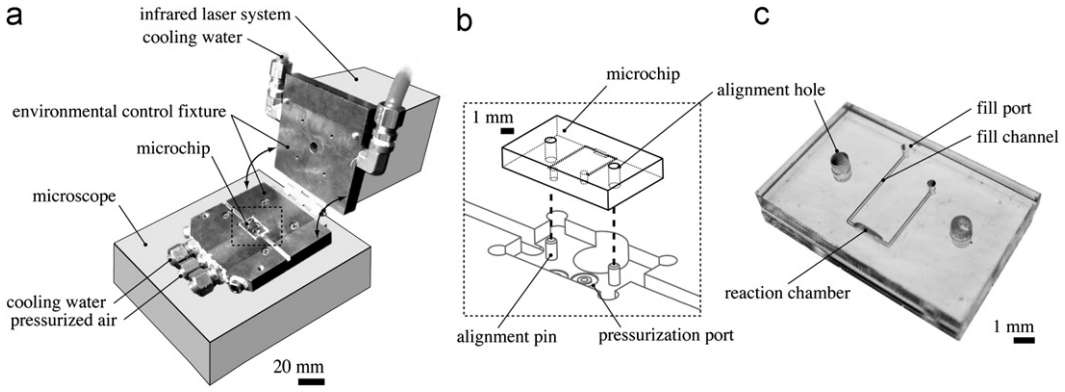

Fig. 1. Photographs (a, c) and diagram (b) of an infrared laser system, environmental control fixture, microchip, and microscope used for rapid, open-loop control of qRT-PCR. (a) The hinged environmental control fixture provides mechanical and thermal repeatability for the microchip and allows microscope and laser access (diagrammed) to the PCR sample. (b) Alignment pins locate the microchip in the base of the fixture. (c) The microchip features a 1 μl reaction chamber with fill channels and ports for loading the PCR sample into the chamber.

chosen to withstand PCR temperatures (95 °C) and pressures (40 psi).

As discussed in previous work (Pak et al., 2012), the microchips were fabricated from laser cut PMMA substrates using a 3-axis vertical milling center (Haas). A machining fixture with a 3×4 array of slots was used to machine up to 12 microchips at once in 5 min (25 s/chip after ~20 min initial setup). All features, including the critical alignment holes and reaction chambers, were milled during the same machining operation (i.e., no re-fixturing required) to ensure accurate relative feature locations. Prior to milling, microchip substrates were binned according to thickness variations of 125 μm to ensure repeatable device fabrication as necessary for open-loop control of PCR. Single bins with common thickness were milled, bonded, and used for a set of experiments. After milling, microchips were cleaned in a 3-stage process that consisted of rinsing with isopropyl alcohol, rinsing with deionized water, and 20 min in an ultrasonic cleaner submerged in deionized water. After cleaning, microchips were blown dry with compressed nitrogen.

Microchips were bonded between clamped, polished tellurium copper plates with alignment pins to align the two halves of the microchip. The plates were polished to a mirror finish to maintain the optical clarity of the PMMA, a requirement for real-time fluorescence detection. For bonding, the plates were placed on a room-temperature hotplate (Corning) and the clamping bolts were tightened to 40 ± 2 in. oz. with a torque screwdriver (Seekonk Precision Tools). The hotplate was then heated to 165 °C for 40 min. After 16 min of bonding time, the bolts were re-tightened to 36 ± 2 in. oz. The temperatures, forces, and times for the bonding process were determined empirically to ensure a strong bond between the two layers of PMMA without significantly deforming any of the milled features.

2.2. Infrared laser PCR system

The laser system consists of a 700 mW 1450 nm infrared laser diode (Hi-Tech Optoelectronics Co.) controlled by a constant current laser driver (Wavelength Electronics), an aspherical collimating lens (Thorlabs) affixed to an *x–y* translational mount (Thorlabs), and a water-cooled tellurium copper heat sink mounted on top of the diode for constant laser power output. The 1450 nm wavelength matches an absorption peak of water while absorption by PMMA is negligible, allowing efficient delivery of radiation without damaging the microchip. The laser heats the aqueous solution in the chamber, with passive cooling via conduction through the chamber walls to the environmental control fixture. The laser system and its initial PCR thermocycling alignment have been described previously (Pak et al., 2012). This alignment process, once performed, does not have to be repeated during normal operation of the machine.

In order to implement open-loop control, a calibration relationship between laser driving voltage and steady state aqueous solution temperature is necessary. We have described this in detail previously (Pak et al., 2012), and summarize it here. A calibration microchip was fabricated with a 125 μm diameter thermocouple (Physitemp) bonded into the reaction chamber along its bottom layer, farthest from the laser. The microchip chamber was filled with water, temperature was measured and bias corrected due to laser heating of the thermocouple. A polynomial was fit to the temperature measurements to generate a calibration curve.

Open-loop control of chamber temperature is effected by driving the laser with a discrete set of voltages without feedback. This voltage input comprises of a series of segments determined uniquely for each temperature transition and subsequent hold: ambient to denaturing, denaturing to annealing, annealing to extension, extension to denaturing, or more generally T_n to T_{n+1}. To determine each segment, we used the known calibration relationship between laser driving voltage, V, and steady state chamber temperature, T, in the following procedure. The laser was driven at V_n corresponding to T_n for 2 min to reach steady state using the calibration microchip in the instrument. V_n was step changed to V_{n+1} corresponding to T_{n+1} for 2 min, again to reach steady state. The temperature $T(t)$ was recorded from the time of the step change for the 2 min duration.

The measured temperature, $T(t)$, was converted to voltages, $V(t)$, using the calibration relationship. For $V_2 > V_1$ (heating), we computed $V_r(t) = 2V_{max} - V(t)$, where V_{max} is the maximum value of $V(t)$, to reflect $V(t)$ about V_{max}. For $V_r(t) > V_{high}$, where V_{high} is the highest voltage that can be safely used for the laser, we set $V_r(t) = V_{high}$. Similarly, for $V_2 < V_1$ (cooling), we computed $V_r(t) = 2V_{min} - V(t)$, where V_{min} is the minimum value of $V(t)$, to reflect $V(t)$ about V_{min}. For $V_r(t) < V_{low}$, where V_{low} is the laser turn-on voltage, we set $V_r(t) = V_{low}$. $V_r(t)$ therefore consists of a constant phase of duration t_c followed by a quasi-exponential phase corresponding to the heating or cooling dynamics of the microchip, an approximately first-order dynamic thermal system. $V_r(t)$ has a 2 min domain. Next $V_r(t)$ is truncated to the duration of $t_c + t_h$, where t_h is the desired hold time for the PCR reaction step. Lastly, the segments are concatenated for the initial denaturing phase and desired number of cycles as required for PCR. This methodology results in a piecewise continuous function, or open-loop laser power profile, consisting of (1) exponentially rising or decaying voltages for temperature holds and (2) maximally on or off voltages for heating or cooling transitions, respectively.

2.3. Environmental control fixture

The environmental control fixture was made up of two hinged 12.7 mm thick tellurium copper plates that were each machined to 80 mm × 80 mm. The base plate, into which the microchip is installed, features a transverse water-cooling passage to control the microchip surface temperature and an air passage to provide 40 psi nitrogen to the microchip fill ports and prevent the expansion of entrained air bubbles during PCR. In the base plate, pressurization ports designed to mate with the microchip fill ports were machined with annular slots for rubber O-rings to seal. A pocket at the center of the base plate designed for a close fit with the microchip ensures an enveloping thermal environment. Alignment pins press fit into the base plate enable accurate and repeatable placement of the microchips in the fixture. To allow the microchip chamber to be imaged for fluorescence detection, an 8 mm hole was drilled through the center of the plate aligned with the center of the reaction chamber. The upper plate, to which the laser system is attached with a cage rod assembly, similarly features a transverse water-cooling passage. To allow the microchip chamber to be heated by the laser system, an 8 mm hole was drilled through the center of the plate aligned with the center of the reaction chamber. Thumbscrews connecting the plates opposite the hinge preload the microchip against the rubber O-rings for operation. The water passages were pumped from a recirculating, temperature-controllable water bath set to 42.8 °C, which impose a microchip chamber temperature of 42 °C.

To assess the mechanical position repeatability of the environmental control fixture, an empty microchip was installed in the fixture on the alignment pins, the fixture was closed and tightened, and the microchip chamber was imaged with a microscope using a 4 × objective (Nikon). A reference line was superimposed over the image and the distance between a chamber sidewall and the reference line was recorded. This measurement was repeated for 10 microchips, each from a different fabrication batch, to determine the error of the positioning of the microchip chamber

along the critical axis of the chamber width, which is most sensitive to misalignment due to the narrow laser beam focal spot. To assess the repeatability of the hinge in positioning the laser over the microchip, small squares of paper printed with solid black toner were cut and taped onto 10 microchips. Each microchip was then placed in the fixture and irradiated with the laser to burn a focal spot onto the paper. Alignment between the focal spot and chamber was then qualitatively verified. To assess thermal stability, a water-filled microchip was placed in the fixture with the laser diode off or on as stated.

2.4. Detection

The laser and environmental chamber assemblies are mounted on top of an inverted microscope (Nikon) as shown in Fig. 1a. A xenon arc lamp (Sutter) filtered to 480/20 nm band-pass was used for the excitation. Emission was filtered (520/20 nm) and imaged with a CCD camera (Roper Scientific) after magnification (4 × /0.2 NA, Nikon). A 3 mm thick water filter, functioning like a hot mirror, was added directly above the microscope objective to absorb any stray infrared radiation and prevent it from damaging the microscope optics. Before running qPCR or qRT-PCR, the water bath, CCD camera, laser driver, and xenon arc lamp were allowed to warm up for 30 min.

For both qPCR and qRT-PCR detection, fluorescence images were collected during the extension phase of every cycle using NIS Elements BR software and post-processed via MATLAB. To avoid photobleaching of the SYBR Green dye, exposure time was limited to 2 s and images were taken 17 s into each extension hold time. The image processing algorithm computed a normalized series of average intensities over a constant region of interest on the microchip, indexed by cycle number. All values below the initial intensity level were set to zero. For qRT-PCR detection, a median filter was applied to smooth fluorescence intensity traces.

For qPCR, three DNA template concentrations ranging from 10^5 to 10^7 starting copies ($n=3$) were amplified to evaluate repeatability and efficiency with known starting template concentrations, providing a standard curve (Fig. 3a). The cycle number threshold, C_T, was set as the cycle number at which the measured fluorescence crosses a threshold of 30σ, where σ is the standard deviation of the fluorescence intensity for the first six PCR cycles.

For qRT-PCR, 5.45 ng of purified mouse embryonic stem cell RNA, as quantified using a Nanodrop spectrophotometer (Thermo Scientific), was used as template for amplification of the GAPDH transcript, which was repeated three times to evaluate repeatability. The cycle number threshold, C_T, was set to 10σ. The RT-PCR products from both the laser thermocycler and conventional, Peltier-based thermocycler (Bio-Rad) controls were evaluated with electrophoresis using an Agilent 2100 Bioanalyzer to determine and compare both the approximate length and final product concentration, or yield, using the DNA 1000 kit that includes sizing and quantification markers at 15 bp and 1500 bp.

Melting curve analysis, or the measurement of the fluorescence of an intercalating dye labeled double stranded DNA solution as it is heated through denaturation, can be used to detect the presence of single-nucleotide polymorphisms (Montgomery et al., 2007; Reed and Wittwer, 2004), and reveal non-specific products (Ririe et al., 1997), and some have used it in the development of microfluidic PCR instrumentation to test temperature accuracy (El-Ali et al., 2004). For melting curve analysis, the microchip was allowed to equilibrate with the environmental control fixture for 5 min after the PCR run was complete. Then, the laser driving voltage was slowly increased from 0.25 V to 0.9 V (20 mW to 500 mW) in 9 min (0.1 °C/s) while fluorescence intensity was measured at 10 Hz. Fluorescence images were post-processed as before, and the rate of change of fluorescence intensity was median filtered and plotted vs. temperature. Signal-to-noise ratio (SNR) was calculated as the difference between the maximum and baseline (constant fluorescence regime at temperatures below melting) divided by the standard deviation of the baseline.

2.5. DNA amplification protocol

For qPCR, a 500 bp amplicon of λ-phage DNA (Affymetrix) was targeted with primer set: 5′-GATGAGTTCGTGTTCGTACAACTGG-3′ and 5′-GGTTATCGAAATCAGCCACAGCGCC-3′. Lyophilized primers (Operon) were re-suspended and diluted into 20 μM aliquots and SYBR Green I dye (Lonza) was used for real-time detection. Reactions were prepared from a commercial master mix, AccuPower PCR PreMix (Bioneer). The premix contained a lyophilized pellet of 2.5 U Top DNA polymerase, 250 μM dNTPs, 10 mM Tris–HCl (pH 9.0), 30 mM KCl, 1.5 mM $MgCl_2$, a tracking dye, and a stabilizer. BSA (Affymetrix) was added to the reaction mix to minimize adsorption of polymerase to the walls of the chamber.

The conventional PCR reactions were prepared according to the following protocol: 11 μl H_2O, 6.0 μl BSA (1 μg/μl), 0.6 μl SYBR Green I (10 ×), 0.4 μl forward and reverse primers (20 μM), and 2.0 μl DNA template (10^5–10^7 starting copies) were added into one 20 μl PCR premix tube. This PCR mix was divided into aliquots of 5 μl, covered with 15 μl of mineral oil (Fisher Scientific), and run on a conventional thermocycler (Bio-Rad) for 40 cycles. A 5 min, 95 °C initial denaturation step was performed at the beginning of cycling and each subsequent cycle consisted of 95 °C for 30 s, 68 °C for 60 s, and 72 °C for 60 s. The last cycle included a 2 min, 72 °C final extension.

Each microfluidic qPCR reaction was prepared from a 2 μl aliquot of the previously prepared PCR mix. To load the PCR reagents into the microchip chambers, 1.5 μl of mineral oil was first loaded into a pipette tip using an adjustable micropipette. The pipettor volume was increased to 2.5 μl and, after carefully bringing the oil interface to the end of the pipette tip, 1 μl of the 2 μl aliquot of PCR solution was loaded. The pipettor volume was then increased to 4 μl and the remaining section of the pipette tip was filled with another plug of mineral oil. This volume is loaded into the microchip, aligning the PCR solution to the reaction chamber. Upon visual observation at 20 × magnification, the oil appears to form a smooth boundary between the droplet and chamber walls, suggesting a fully encapsulating passivation layer between them to mitigate adsorption of the polymerase to the polymer chamber walls (Phaneuf et al., 2012). A total of 30 cycles were performed, with a 1 min initial denaturation for the first cycle and all subsequent cycles consisted of 93 °C for 10 s, 68 °C for 20 s, and 72 °C for 20 s.

2.6. RNA amplification protocol

For qRT-PCR, a 100 base segment of the RNA transcript from the GAPDH housekeeping gene was chosen as the target using the following primer set: 5′-GCCTTCCGTGTTCCTACC-3′ and 5′-GCCTGCTTCACCACCTTC-3′. GAPDH was chosen for its consistent expression during stem cell differentiation as a control for thermocycler validation. Total RNA was extracted from mouse embryonic stem cell culture lysate. Lyophilized primers were re-suspended and diluted into 10 μM aliquots according to the manufacturer's protocol. AccuPower one-step RT-PCR PreMix tubes were used for the reaction premix, capable of single tube reverse transcription and PCR, and SYBR Green I dye was used for real-time detection. BSA was added to the reaction to minimize adsorption of polymerase to the walls of the chamber.

The conventional RT-PCR reactions were prepared according to the following protocol: 14.1 μl H_2O, 3.0 μl BSA (1 μg/μl), 0.40 μl SYBR Green I (10 ×), 0.75 μl forward primer (10 μM), 0.75 μl

reverse primer (10 μM), and 1.0 μl RNA template (109 ng/μl) were added into one 20 μl RT-PCR premix tube. This PCR mix was divided into aliquots of 5 μl, covered with 15 μl of mineral oil, and run on a conventional thermocycler. The sample was first held at 42 °C for 60 min for the reverse transcription process followed by 40 PCR cycles. A 5 min, 94 °C initial denaturation step was included at the beginning and each subsequent cycle consisted of 94 °C for 10 s, 56 °C for 30 s, and 72 °C for 30 s.

Each microfluidic qRT-PCR reaction was prepared from a 2 μl aliquot of the previously prepared RT-PCR mix. Pipettes were filled according to the same process described above in Section 2.5. The microchip was installed in the fixture at 42 °C for 30 min with the laser off to allow the reverse transcription to occur prior to thermocycling. A total of 30 cycles were performed, with a 1 min denaturation for the first cycle to inactivate the reverse transcriptase and denature the cDNA and all subsequent cycles consisted of 93 °C for 10 s, 56 °C for 20 s, and 72 °C for 20 s. Both the PCR and RT-PCR recipes utilize common reagent concentrations, unlike most reported microfluidic PCR that require 2–20 × more, due to our passivation method.

3. Results and discussion

3.1. Mechanical and thermal performance

The microchip fabrication process and environmental control fixture were designed to maximize mechanical repeatability, essential for open-loop controlled PCR and RT-PCR. The combined processes of milling, bonding, and installing the microchip were measured with microscopy to be within ±15 μm total range, corresponding to 3% of the microchip chamber width, along the critical axis of the chamber width ($n=10$).

The environmental control fixture provides exceptional thermal stability. For the reverse transcription step with set point of 42 °C, with the laser diode off, we measured chamber temperature accuracy of 0.29 °C (average difference from the set point), with precision represented by the standard deviation of 0.09 °C.

We next evaluated the accuracy and precision of the system over the course of 20 consecutive cycles for both PCR and RT-PCR, representing one thermocycling run. The accuracy was computed as difference between the set point and measured average temperature at each of the three set points (denaturing, annealing, and extension). In this calculation, the measured average temperature is defined as the average temperature during 20 10 s intervals, consecutively, one per cycle. We then computed the precision, similarly, as the average of the measured temperature variation at each of the three set points. We define the measured temperature variation as the standard deviation of the temperature over 20 10 s intervals, consecutively, one per cycle. For PCR, the accuracy was 0.12 °C, 0.82 °C, and 0.53 °C and precision was 0.16 °C, 0.18 °C, and 0.15 °C for the denaturing, annealing, and extension steps, respectively. For RT-PCR, the accuracy was 0.59 °C, 0.12 °C, and 0.02 °C and precision was 0.21 °C, 0.41 °C, and 0.25 °C for the denaturing, annealing, and extension steps, respectively.

Lastly, we evaluated the run-to-run variability as a measure of repeatability. After computing the measured average temperature at each of the three set points for two different runs, we took the pairwise difference between them and averaged these three differences (one per set point). The run-to-run variability for PCR was 0.12 °C; for RT-PCR it was 0.31 °C.

The open-loop laser power profile and resulting microchip chamber temperature as calculated from calibration are shown in Fig. 2 for PCR. The chamber temperature rapidly and repeatably reaches each stable hold phase with minimal overshoot.

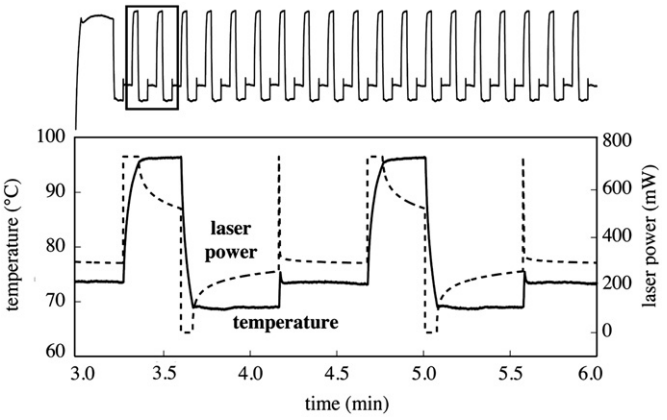

Fig. 2. Open-loop laser power profile (dashed) and corresponding microchip chamber temperature (solid) for microfluidic PCR. This profile was determined from a calibration between laser driving voltage, laser output power, and chamber temperature, along with characterization of temperature dynamics during temperature transitions and holds. This temperature profile was used to perform qPCR of a 500 bp amplicon of λ-phage DNA for 30 cycles, with a 1 min initial denaturation for the first cycle and all subsequent cycles consisting of 93 °C for 10 s, 68 °C for 20 s, and 72 °C for 20 s.

This temperature stability is comparable to those reported by other conventional and microfluidic PCR systems. Conventional thermoelectric instruments (e.g., Bio-Rad MJ Mini) achieve temperature uniformity, or precision, of around 0.4 °C. The Roche Light-Cycler reports temperature uniformity up to 0.15 °C (Lee et al., 2010). One recent microfluidic PCR system, by Angione et al. (2012) reported temperature variations for the reverse-transcription, annealing, and extension steps of 0.8 °C, 0.1 °C, and 1.3 °C, respectively.

3.2. Quantitative PCR and RT-PCR

Efficiency, sensitivity, specificity, accuracy and reproducibility are all important factors when comparing a novel PCR assay to traditional laboratory equipment (van Pelt-Verkuil et al., 2008). To evaluate the system, real-time amplifications of both DNA and RNA were performed as shown in Fig. 3.

The logarithms of the λ-phage DNA starting copy numbers were plotted against cycle threshold values, and a linear regression fit was performed. The coefficient of determination, R^2, from this regression analysis was 0.9933. The standard deviations of these cycle threshold values were computed as 0.5, 1.2, and 0.5 cycles for 10^5, 10^6, and 10^7 starting copies, respectively, indicating good repeatability.

The efficiency, E, of the system was calculated from the slope of the standard curve ($k=-5.1$) and found to be $E=100(10^{-1/k}-1)=57\%$. Conventional PCR systems typically achieve 65–90% (Schefe et al., 2006; Tichopad et al., 2003), and microfluidic PCR systems typically report lower efficiencies due primarily to high surface-area-to-volume-ratio and the resulting adverse surface interactions (Zhang and Xing, 2007; Zhang et al., 2006). Ours is somewhat lower than those of conventional systems, perhaps due to non-optimal reagent concentrations, cycle hold times, or temperatures, but amplification was obtained consistently for both DNA and RNA. The repeatability of the qRT-PCR was also measured by calculating the standard deviation of the C_T values and found to be 1.0 cycle.

For PCR amplification of λ-phage DNA, 30 cycles took 35 min total. For RT-PCR amplification of GAPDH, an initial 30 min was allotted for reverse transcription, resulting in a total time of 65 min.

The average heating and cooling rates of the system were 3.3 °C/s and 3.86 °C/s, respectively. Conventional thermoelectric qPCR thermocyclers (e.g., Bio-Rad MJ Mini) operate with heating

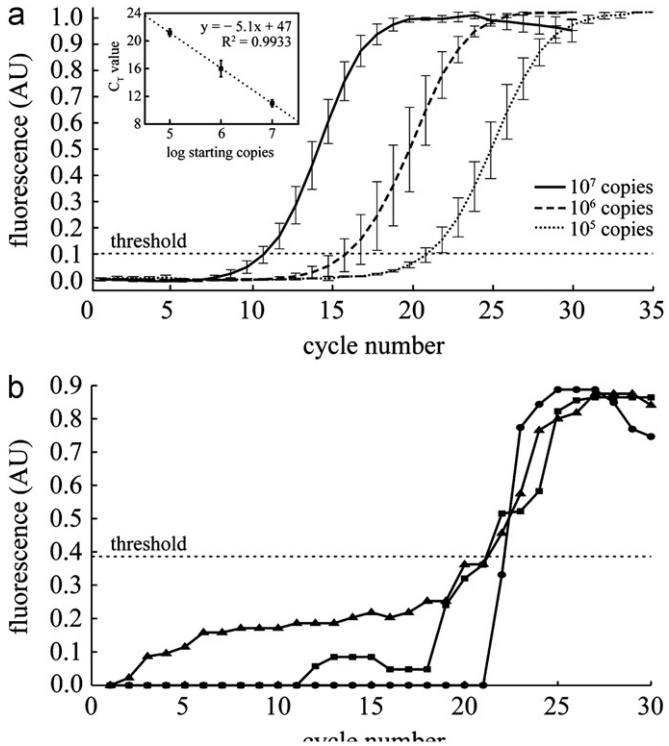

Fig. 3. Fluorescence intensity vs. cycle number for qPCR and qRT-PCR. (a) PCR of λ-phage DNA with varying starting copies showing accurate exponential amplification of serial dilutions. The inset shows C_T vs. log starting copy number, used to determine amplification efficiency. Each data point represents the average of three replicates, with error bars corresponding to one standard deviation. (b) RT-PCR of GAPDH RNA transcript for three trials showing repeatable cycle number threshold for amplification. PCR λ-phage DNA required 35 min for 30 cycles; RT-PCR of GAPDH required 65 min considering an initial 30 min for reverse transcription.

and cooling rates of 3.3 °C/s and 2.0 °C/s while the Roche Light-Cycler qPCR instrument reports heating and cooling rates of 3.3 °C/s and 3.0 °C/s (Lee et al., 2010). One recent microfluidic qPCR system by Angione et al. (2012) reported heating and cooling rates of 1.6 °C/s and 1.8 °C/s. A more rapid microfluidic qPCR capable system (Yu et al., 2012) reports achieving 30 cycles in 26 min (rates were not reported) as compared to our 30 cycles in 35 min, and Kim et al. (2009) achieve 40 cycles in 6 min.

Comparatively, of the thermocyclers capable of qPCR, our system is faster than conventional thermocyclers and most microfluidic qPCR thermocyclers. The speed is comparable to that of the Roche Light-cycler, but with smaller volumes (1 μl vs. 10–50 μl) and potential for integration of multiple pre- and post-PCR steps as others have done (Easley et al., 2006; Legendre et al., 2006). Compared to faster microfluidic qPCR systems (Kim et al., 2009; Yu et al., 2012), our system is capable of RT-qPCR in addition to qPCR, uses disposable polymer microchips, and is easier to use (e.g., does not require thermocouple insertion into the microfluidic device). Although we have previously used a version of this system to perform faster PCR (e.g., 10 min/analysis), the design reported here exhibits slower cooling rates due to the environmental control fixture and therefore longer analysis time.

3.3. End-point analysis

End-point detection analysis was used to compare the PCR and RT-PCR yields and specificity of the laser thermocycler and conventional thermocycler, shown in Fig. 4. Yields from PCR were not statistically different ($P=0.5823$; t-test), nor were yields from RT-PCR ($P=0.8672$; t-test).

Regarding specificity, electropherogram results indicate that the formation of non-specific PCR products was reduced with the laser thermocycler. In contrast to other reports suggesting the presence of non-specific products during microfluidic qPCR of DNA (Yu et al., 2012), we did not observe this (Fig. 4a,b). The laser thermocycler yields slightly improved performance of qRT-PCR of RNA as compared to a conventional thermocycler (Fig. 4c,d).

The melting curve analysis, in which the rate of change in florescence is plotted against temperature, is shown in Fig. 5. The λ-phage amplicon melted at 84.5 °C, corresponding to the maximum value of the rate of change in fluorescence. This agrees well with the melting temperature of 85.5 °C as measured with a conventional qPCR instrument (Applied Biosystems StepOnePlus Sequence Detector).

In contrast to other microfluidic qPCR instrumentation (Yu et al., 2012), our instrument is able to directly measure the melting curve following amplification, and has higher signal-to-noise ratio (SNR), 46 vs. 12. Despite the lower efficiency of the laser thermocycler, the specificity, as evidenced by Fig. 4, and sensitivity, evidenced by our limit of detection studies with 30 cycles (Phaneuf et al., 2012), are either comparable or superior to those of conventional PCR.

4. Conclusions

We report a microfluidic qRT-PCR instrument capable of gene expression measurement in an easy-to-use format in approximately 1 h. The disposable polymer microchip is low-cost and more rapidly fabricated at relevant quantities (tens to thousands) than comparable glass or silicon devices (Becker and Gärtner, 2008). An environmental control fixture provides mechanical and thermal repeatability for an infrared laser to achieve open-loop temperature control of 1 μl reaction volumes in a low-cost polymer microfluidic chip with concurrent fluorescent imaging. For both DNA and RNA qPCR, detection results were accurate, repeatable, with efficiency of 57%, and showed comparable yield and improved specificity over those conventional methods. Melting curve analysis validated the accuracy of the amplification products. We note that this reported instrument is not capable of gene expression analysis of multiple transcripts simultaneously or single cell gene expression measurement. Yet, in emerging

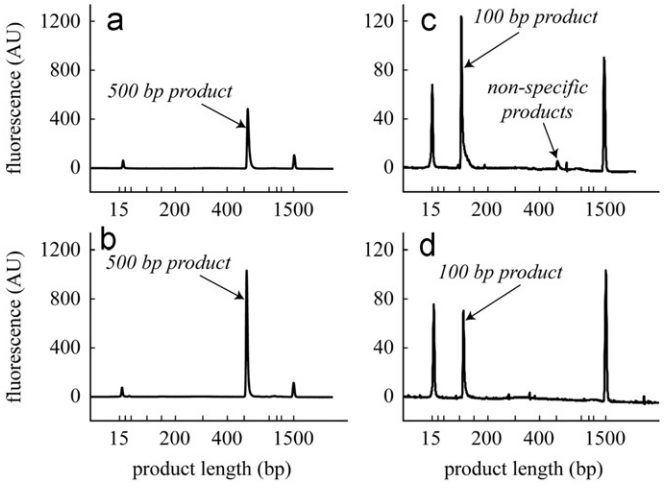

Fig. 4. Representative electropherograms of PCR of λ-phage DNA (a, b) and RT-PCR of GAPDH RNA transcript (c, d) products using both a conventional thermocycler with 5 μl volume (a, c) and laser thermocycler with 1 μl microchip chamber (b, d). The microfluidic PCR system shows comparable yield and improved specificity. Outer peaks correspond to sizing and quantification markers (15 bp and 1500 bp).

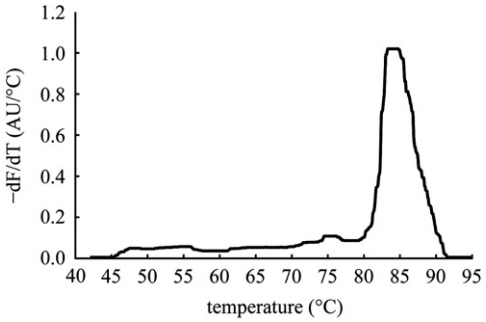

Fig. 5. Melting curve analysis of the λ-phage amplicon. The melting temperature is the temperature that produced the largest rate of change in fluorescence, 84.5 °C, agreeing with measurement by conventional qPCR instrumentation.

fields such as stem cell biomanufacturing (Nair et al., 2012), where gene expression is tracked over time cell populations and expression levels change from environmental stimuli in minutes to hours (Stahlberg and Bengtsson, 2010; Yosef and Regev, 2011), or during differentiation from hours to days, rapid, microfluidic qRT-PCR could be a tool of real-time monitoring and control.

Acknowledgements

We acknowledge funding from NSF (EHR 0965945), Centers for Disease Control, Georgia Tech Translational Research Institute for Biomedical Engineering and Science (TRIBES) Seed Grant Awards Program and support from Georgia Tech through the Institute for Bioengineering and Biosciences Junior Faculty Award, Technology Fee Fund, Invention Studio, and the George W. Woodruff School of Mechanical Engineering. We would like to acknowledge Stephen Culpepper, Mark McJunkin, and Marty Jacobson for their assistance with fabrication and machine shop training. This research was performed under an appointment to the Department of Homeland Security (DHS) Scholarship and Fellowship Program, administered by the Oak Ridge Institute for Science and Education (ORISE) through an interagency agreement between the US Department of Energy (DOE) and DHS. ORISE is managed by Oak Ridge Associated Universities (ORAU) under DOE Contract no. DE-AC05-06OR23100. All opinions expressed in this paper are those of the authors and do not necessarily reflect the policies and views of DHS, DOE, or ORAU/ORISE.

References

Anon., Nature Biotechnology 24 (9), 2006, 1039. 〈http://www.nature.com/nbt/journal/v24/n9/full/nbt0906-1039.html〉.
Angione, S., Chauhan, A., Tripathi, A., 2012. Analytical Chemistry 84 (6), 2654–2661.
Bao, G., Rhee, W.J., Tsourkas, A., 2009. Annual Review of Biomedical Engineering 11, 25–47.
Becker, H., Gärtner, C., 2008. Analytical and Bioanalytical Chemistry 390 (1), 89–111.
Boyer, L.A., Lee, T.I., Cole, M.F., Johnstone, S.E., Levine, S.S., Zucker, J.P., Guenther, M.G., Kumar, R.M., Murray, H.L., Jenner, R.G., Gifford, D.K., Melton, D.A., Jaenisch, R., Young, R.A., 2005. Cell 122 (6), 947–956.
Cao, Q., Mahalanabis, M., Chang, J., Carey, B., Hsieh, C., Stanley, A., Odell, C.A., Mitchell, P., Feldman, J., Pollock, N.R., Klapperich, C.M., 2012. PLOS ONE 7 (3), e33176.
Dahl, A., Sultan, M., Jung, A., Schwartz, R., Lange, M., Steinwand, M., Livak, K., Lehrach, H., Nyarsik, L., 2007. Biomedical Microdevices 9 (3), 307–314.
Easley, C.J., Karlinsey, J.M., Bienvenue, J.M., Legendre, L.A., Roper, M.G., Feldman, S.H., Landers, J.P., 2006. Proceedings of the National Academy of Sciences of the United States of America 103 (51), 19272–19277.
El-Ali, J., Perch-Nielsen, I.R., Poulsen, C.R., Bang, D.D., Telleman, P., Wolff, A., 2004. Sensors and Actuators A: Physical 110 (1Âi3), 3–10.
Erlich, H.A., Gelfand, D., Sninsky, J.J., 1991. Science 252 (5013), 1643–1651.
Hua, Z., Rouse, J.L., Eckhardt, A.E., Srinivasan, V., Pamula, V.K., Schell, W.A., Benton, J.L., Mitchell, T.G., Pollack, M.G., 2010. Analytical Chemistry 82 (6), 2310–2316.
Huhmer, A.F.R., Landers, J.P., 2000. Analytical Chemistry 72 (21), 5507–5512.
Itzkovitz, S., van Oudenaarden, A., 2011. Nature Methods 8 (Suppl. 4s), 512–519.
Kaigala, G.V., Hoang, V.N., Stickel, A., Lauzon, J., Manage, D., Pilarski, L.M., Backhouse, C.J, 2008. Analyst 133 (3), 331–338.
Kim, H., Vishniakou, S., Faris, G.W., 2009. Lab on a Chip 9 (9), 1230–1235.
Lee, D., Chen, P., Lee, G., 2010. Biosensors and Bioelectronics 25, 1820–1824.
Legendre, L.A., Bienvenue, J.M., Roper, M.G., Ferrance, J.P., Landers, J.P., 2006. Analytical Chemistry 78 (5), 1444–1451.
Liang, P., 2007. Nature Biotechnology 25 (1), 27–28.
Lien, K.-Y., Lee, W.-C., Lei, H.-Y., Lee, G.-B., 2007. Biosensors and Bioelectronics 22 (8), 1739–1748.
Liu, P., Seo, T.S., Beyor, N., Shin, K.-J., Scherer, J.R., Mathies, R.A., 2007. Analytical Chemistry 79 (5), 1881–1889.
Lopez-Maury, L., Marguerat, S., Bahler, J., 2008. Nature Reviews Genetics 9 (8), 583–593.
Malone, J.H., Oliver, B., 2011. BMC Biology 9 (34), 1–9.
Montgomery, J., Wittwer, C.T., Palais, R., Zhou, L., 2007. Nature Protocol 2 (1), 59–66.
Nair, R., Ngangan, A.V., Kemp, M.L., McDevitt, T.C., 2012. 7 (10), 2012, e42580.
Neuzil P., Zhang C., Pipper J., Oh S. and Zhuo L., Nucleic Acids Research 34 (11), 2006, e77. 〈http://nar.oxfordjournals.org/content/34/11/e77〉.
Oosterbroek, R.E., Berg, A., 2003. Elsevier.
Pak, N., Saunders, D.C., Phaneuf, C.R., Forest, C.R., 2012. Biomedical Microdevices 14, 427–433.
Phaneuf, C., Oh, K., Pak, N., Saunders, D., Conrardy, C., Landers, J., Tong, S., Forest, C., 2012. Biomedical Microdevices, 1–11.
Phaneuf, C.R., Pak, N., Forest, C.R., 2011. Sensors and Actuators A: Physical 167 (2), 531–536.
Reed, G.H., Wittwer, C.T., 2004. Clinical Chemistry 50 (10), 1748–1754.
Ririe, K.M., Rasmussen, R.P., Wittwer, C.T., 1997. Analytical Biochemistry 245 (2), 154–160.
Sanchez-Freire, V., Ebert, A., Kalisky, T., Quake, S., Wu, J., 2012. Nature Protocols 7 (5), 829–838.
Santangelo, P., Lifland, A., Curt, P., Sasaki, Y., Bassell, G., Lindquist, M., Crowe, J., 2009. Nature Methods 6 (5), 347–349.
Santangelo, P., Nix, B., Tsourkas, A., Bao, G., 2004. Nucleic Acids Research 32 (6), e57.
Schefe, J., Lehmann, K., Buschmann, I., Unger, T., Funke-Kaiser, H., 2006. Journal of Molecular Medicine 84 (11), 901–910.
Schena, M., Shalon, D., Davis, R.W., Brown, P.O., 1995. Science 270, 467–470.
Sperger, J.M., Chen, X., Draper, J.S., Antosiewicz, J.E., Chon, C.H., Jones, S.B., Brooks, J.D., Andrews, P.W., Brown, P.O., Thomson, J.A., 2003. Proceedings of the National Academy of Sciences of the United States of America 100 (23), 13350–13355.
Spurgeon, S.L., Jones, R.C., Ramakrishnan, R., 2008. PLOS ONE 3 (2), e1662.
Stahlberg, A., Bengtsson, M., 2010. Methods 50, 282–288.
Tichopad A., Dilger M., Schwarz G. and Pfaffl M.W., Nucleic Acids Research 31 (20), 2003, e122. 〈http://www.ncbi.nlm.nih.gov/pmc/articles/pmc219490〉.
van Pelt-Verkuil, E., van Belkum, A., Hays, J.P., 2008. Springer.
Warren, L., Bryder, D., Weissman, I.L., Quake, S.R., 2006. Proceedings of the National Academy of Sciences of the United States of America 103 (47), 17807–17812.
White, A.V., Petriv, M., Hamidi, O., Sikorski, M., Marra, D., Piret, M., Aparicio, J., Hansen, C., S., 2011. Proceedings of the National Academy of Sciences of the United States of America 108 (34), 13999–14004.
Wittwer, C.T., Ririe, K.M., Andrew, R.V., David, D.A., Gundry, R.A., Balis, U.J., 1997. BioTechniques 22 (1), 176–181.
Wooley, A.T., Hadley, D., Landre, P., de Mello, A.J., Mathies, R.A., Northrup, M.A., 1996. Analytical Chemistry 68 (23), 4081–4086.
Yosef N. and Regev A., Cell 144 (6), 2011, 886–896. 〈http://www.cell.com/abstract/S0092-8674(11)00129-2〉.
Yu, Y., Li, B., Baker, C.A., Zhang, X., Roper, M.G., 2012. Analytical Chemistry 84 (6), 2825–2829.
Zare, R., Kim, S., 2010. Annual Review of Biomedical Engineering 12, 187–201.
Zeng, Y., Novak, R., Shuga, J., Smith, M., Mathies, R., 2010. Analytical Chemistry 82 (8), 3183–3190.
Zhang, C., Xing, D., 2007. Nucleic Acids Research 35 (13), 4223–4237.
Zhang, C., Xu, J., Ma, W., Zheng, W., 2006. Biotechnology Advances 24 (3), 243–284.
Zhong, J., Chen, Y., Marcus, J., Scherer, A., Quake, S., Taylor, C., Weiner, L., 2007. Lab on a Chip 8, 68–74.
Zhong, J., Feng, Y., Taylor, C., 2008. Current Medicinal Chemistry 15 (28), 2897–2900.